Suppression of emittance variation in extremely low emittance light source storage rings

Toshihiko Hiraiwa,[1] Kouichi Soutome,[2,1] and Hitoshi Tanaka[1,*]

[1]*RIKEN SPring-8 Center (RSC), Sayo, Hyogo 679-5148, Japan*

[2]*Japan Synchrotron Radiation Research Institute (JASRI), Sayo, Hyogo 679-5198, Japan*

(Received 8 December 2021; accepted 28 March 2022; published 26 April 2022)

A passive method based on an optimized quasiachromatic condition effectively suppresses emittance variation during the independent tuning of insertion devices (IDs), which is one of the major obstacles for conducting precise experiments in extremely low emittance light source storage rings. This method, simple and easy to apply to any light source storage ring, reduces the emittance variation to potentially less than 1% by carefully optimizing dispersion leakage at the straight sections where the IDs are installed according to an actual condition of the ID independent tuning.

DOI: 10.1103/PhysRevAccelBeams.25.040703

I. INTRODUCTION

In extremely low emittance light source storage rings with an emittance less than a few hundred pmrad, a multibend achromat (MBA) lattice is used to achieve extremely small emittance values [1,2], and the straight sections where insertion devices (IDs) such as undulators and wigglers are installed are designed to be free from linear energy dispersion. The main reason for the straight section to be dispersion-free is that the finite energy dispersion at the light source point increases the source size in the horizontal direction due to the energy spread, which, in turn, leads to a non-negligible degradation of brilliance for the ring with emittance less than a few hundred pmrad.

In storage rings with an MBA lattice structure, the average magnetic field of the bending magnets is generally lower than that of conventional third-generation light source storage rings in order to reduce the emittance value as close as possible to its lower limit; hence, the contribution of the radiation from the IDs to radiation damping becomes relatively large. In third-generation light source storage rings, independent tuning has been established as a standard operational mode for user experiments, where the ID parameters at each beam line are adjusted from time to time according to the specific requirements of each experiment. The opening and closing of the ID gaps carried out during the independent tuning significantly change the integral field on the axis. This results in changing both the radiation damping of the ring and the emittance. Consequently, the emittance varies greatly, changing the brightness of the undulator radiation and presenting substantial problems for conducting precision experiments in extremely low emittance light sources [3].

One possible solution is to build an emittance control system combining a damping wiggler [4] with a real-time emittance monitor [5–7] in the ring to maintain constant emittance by adjusting radiation damping [3,8–9]. With this method, the damping wiggler must be long enough to offset the amount of change in radiation damping due to the opening and closing of the ID gaps in the user experiment. Then, if the ring circumference is to remain unchanged, the number of ID beam lines available for user experiments must be reduced, and if the same number of beam lines is to be maintained, the ring circumference would have to be increased.

In this paper, we propose a passive method to solve this problem without introducing extra damping wigglers into the ring. The method we propose is to leak a small amount of linear dispersion into each straight section where an ID is installed and to optimize the amount of dispersion leakage so that the variation in emittance due to the opening and closing of the ID gaps is minimized by balancing the radiation excitation and damping caused by IDs. In third-generation light source storage rings, the linear dispersion leakage from the arc to the straight section has been optimized to reduce the emittance of the ring [10]. In this case, the amount of dispersion leakage is significant, 10 cm or more. On the other hand, to compensate for emittance variation in extremely low emittance light source storage rings, the necessary leakage of the linear dispersion is substantially smaller, only 1 cm or less, and the condition is considered quasiachromatic.

*Corresponding author.
tanaka@spring8.or.jp

In the following section, the optimum quasiachromatic condition is formulated, which minimizes the variation of the effective emittance under a given condition of the independent tuning. In Sec. III, the derived formula is applied to an actual case for its validation. In Sec. IV, the proposed scheme is also investigated to evaluate effectiveness of the scheme under various ring and operational conditions. Finally, the results and conclusion are summarized in Sec. V.

II. FORMULATION OF THE OPTIMUM QUASIACHROMATIC CONDITION TO REDUCE EMITTANCE VARIATION

In this section, we optimize the linear dispersion leakage value at the straight section where the ID is installed. Optimization is performed so that the changes in radiation excitation and damping due to the opening and closing of the ID gaps cancel each other out, and the change in the effective emittance is minimized over the ID operating range. Since the brilliance is inversely proportional to the effective emittance, this procedure also reduces the variation of the brilliance. Of course, a small dispersion leakage caused by this method will increase the beam size at straight sections, resulting in at most a 15%–20% reduction of the brilliance, but can instead reduce the variation of the brilliance during an user operation period down to about 6% or less.

To determine the ID operating range, we introduce the concept of average ID peak field over the ring as an indicator, which is obtained by integrating the peak magnetic field of each ID depending on the gap closing state. The large number of gap closing states over all of the beam lines makes it difficult to treat them individually. The concept of the average ID peak field allows us to represent all the gap closing states by a single parameter. Note that this treatment is valid, because radiation damping is determined by the magnetic field on the axis integrated over the ring. The effective emittance $\varepsilon_{\mathrm{eff}}(s) \equiv \varepsilon_{x,\mathrm{eff}}(s)$, including the contribution of the dispersion, is given by [10]

$$\begin{aligned}\varepsilon_{\mathrm{eff}}(s) = \{&[\beta_x(s)\varepsilon_x + \eta_x(s)^2\sigma_\delta^2] \times [\gamma_x(s)\varepsilon_x + \eta_x'(s)^2\sigma_\delta^2] \\ &- [-\alpha_x(s)\varepsilon_x + \eta_x(s)\eta_x'(s)\sigma_\delta^2]^2\}^{1/2}, \end{aligned} \tag{1}$$

where $\beta_x(s)$, $\alpha_x(s)$, and $\gamma_x(s) \equiv \frac{1+\alpha_x^2(s)}{\beta_x(s)}$ are the Twiss parameters at position s along the electron beam orbit, $\eta_x(s)$ and $\eta_x'(s)$ are the linear dispersion function and its derivative with respect to s, respectively, and ε_x and σ_δ denote the natural emittance and relative energy spread, respectively. Since the beta function distortion and the energy dispersion generated by IDs are expected to be negligible, we ignore them here. We further assume that $\eta_x'(s) = 0$ in the straight section where the ID is installed and that $\alpha_x(s)$ is also zero at the center of the straight section. With these assumptions, Eq. (1) can be simplified as follows:

$$\varepsilon_{\mathrm{eff}}(s) = [{\varepsilon_x}^2 + \gamma_x(s)\eta_x(s)^2\varepsilon_x\sigma_\delta^2]^{1/2}. \tag{2}$$

Let us consider balancing the radiation excitation and damping due to the opening and closing of the ID gaps, by breaking the achromatic condition to leak a very small amount of dispersion into the straight section. Since the leaked dispersion is small, we neglect changes in emittance and relative energy spread due to optics tuning and also assume that the natural emittance ε_{x0} and relative energy spread $\sigma_{\delta 0}$ determined only by bending magnets are independent of this small dispersion leakage. The contribution of the dispersion generated by the undulator (with a small K value) itself is insignificant as well, so we ignore it here to simplify the formulation. With these assumptions and further assuming a purely sinusoidal ID field, ε_x and σ_δ can be written as follows using the Twiss parameter and the dispersion function in the straight section:

$$\varepsilon_x = \frac{C_q\gamma^2}{J_x}\frac{I_5 + \Delta I_5}{I_2 + \Delta I_2}, \tag{3}$$

$$\varepsilon_{x0} = \frac{C_q\gamma^2}{J_{x0}}\frac{I_5}{I_2}, \tag{4}$$

$${\sigma_\delta}^2 = \frac{C_q\gamma^2}{J_E}\frac{I_3 + \Delta I_3}{I_2 + \Delta I_2}, \tag{5}$$

$${\sigma_{\delta 0}}^2 = \frac{C_q\gamma^2}{J_{E0}}\frac{I_3}{I_2}, \tag{6}$$

where

$$I_2 \equiv \oint_{\mathrm{BM}} \frac{ds}{\rho(s)^2} = \sum_{i=1}^{N_{\mathrm{BM}}} \frac{\Delta_i}{\rho_{\mathrm{BM},i}}, \tag{7}$$

$$I_3 \equiv \int_{\mathrm{BM}} \frac{ds}{|\rho(s)^3|} = \sum_{i=1}^{N_{\mathrm{BM}}} \frac{\Delta_i}{\rho_{\mathrm{BM},i}^2}, \tag{8}$$

$$I_4 \equiv \oint_{\mathrm{BM}} \left\{\frac{\eta_x(s)}{\rho(s)^3} + \frac{2K(s)\eta_x(s)}{\rho(s)}\right\} ds, \tag{9}$$

$$I_5 \equiv \oint_{\mathrm{BM}} \frac{H(s)}{|\rho(s)|^3}\, ds \tag{10}$$

are the radiation integrals for the bare ring without IDs,

$$\Delta I_2 = \sum_{i=1}^{N_{\mathrm{ID}}} \frac{L_{\mathrm{ID},i}}{2\rho_{\mathrm{ID},i}^2}, \tag{11}$$

$$\Delta I_3 = \frac{4}{3\pi}\sum_{i=1}^{N_{\mathrm{ID}}} \frac{L_{\mathrm{ID},i}}{\rho_{\mathrm{ID},i}^3}, \tag{12}$$

$$\Delta I_4 \cong 0, \tag{13}$$

$$\Delta I_5 = \oint_{\mathrm{ID}} \frac{H(s)}{|\rho(s)|^3} \tag{14}$$

are the amount of their changes by IDs,

$$J_{x0} = 1 - \frac{I_4}{I_2}, \tag{15}$$

$$J_x \cong 1 - \frac{I_4}{I_2 + \Delta I_2} = J_{x0} \frac{I_2 + \frac{1}{J_{x0}} \Delta I_2}{I_2 + \Delta I_2}, \tag{16}$$

$$J_{E0} = 2 + \frac{I_4}{I_2}, \tag{17}$$

$$J_E \cong 2 + \frac{I_4}{I_2 + \Delta I_2} = J_{E0} \frac{I_2 + \frac{2}{J_{E0}} \Delta I_2}{I_2 + \Delta I_2} \tag{18}$$

are the horizontal and longitudinal damping partition numbers without and with IDs, and

$$H(s) \equiv \gamma_x(s)\eta_x(s)^2 + 2\alpha_x(s)\eta_x(s)\eta_x'(s) + \beta_x(s)\eta_x'(s)^2, \tag{19}$$

$$\sum_{i=1}^{N_{\mathrm{BM}}} \Delta_i = 2\pi. \tag{20}$$

In the above equations, $C_q = 3.8319 \times 10^{-13}$ m is the quantum fluctuation coefficient, γ the Lorentz factor, $\rho(s)$ the radius of curvature at the position s, $K(s)$ the strength of quadrupole field, N_B the number of bending magnets taking into account the number of divisions of the longitudinal gradient bend if it is used, $\rho_{\mathrm{BM},i}$ and Δ_i the radius of curvature and the bending angle, respectively, of the ith bending magnet, N_{ID} the number of IDs, $L_{\mathrm{ID},i}$ the length of the ith ID, and $\rho_{\mathrm{ID},i}$ its radius of curvature corresponding to the peak magnetic field. Note that, with the dispersion leakage considered here, the contribution to I_4 from IDs is several orders of magnitude smaller than that from bending magnets and hence is neglected [Eq. (13)].

Now we further simplify $\oint_{\mathrm{ID}} \frac{H(s)}{|\rho(s)|^3}$. As mentioned above, we assume $\eta_x'(s) = 0$ in the straight section, and, hence, the dispersion here takes a constant value $\eta_x(s) = \eta_{x\_\mathrm{ST}}$. If we denote the minimum value of the beta function in the straight section as $\beta_{\mathrm{ID\_min}}$, the integral can be specified as follows:

$$\oint_{\mathrm{ID}} \frac{H(s)}{|\rho(s)|^3} = \oint_{\mathrm{ID}} \frac{\frac{\eta_{x\_\mathrm{ST}}{}^2}{\beta_{\mathrm{ID\_min}}}}{|\rho(s)|^3} = \frac{4}{3\pi} \frac{\eta_{x\_\mathrm{ST}}{}^2}{\beta_{\mathrm{ID\_min}}} \sum_{i=1}^{N_{\mathrm{ID}}} \frac{L_{\mathrm{ID},i}}{\rho_{\mathrm{ID},i}^3}. \tag{21}$$

Note that this expression holds even if the waist position of the beta function is not at the ID center. Using Eq. (21), the emittance ε_x can be expressed as

$$\varepsilon_x = \frac{C_q \gamma^2}{J_{x0}} \frac{I_5 + \frac{4}{3\pi} \frac{\eta_{x\_\mathrm{ST}}{}^2}{\beta_{\mathrm{ID\_min}}} \sum_{i=1}^{N_{\mathrm{ID}}} \frac{L_{\mathrm{ID},i}}{\rho_{\mathrm{ID},i}^3}}{I_2 + \frac{1}{J_{x0}} \sum_{i=1}^{N_{\mathrm{ID}}} \frac{L_{\mathrm{ID},i}}{2\rho_{\mathrm{ID},i}^2}}. \tag{22}$$

To simplify the equation of the effective emittance, the radius of curvature $\rho_{\mathrm{ID},i}$ is approximated by the simple average value ρ_{ID}, and the same length L_{ID} is used for all IDs. We then have

$$\varepsilon_{\mathrm{eff}}@\mathrm{ID\_ST} = \left(\varepsilon_x{}^2 + \frac{\eta_{x\_\mathrm{ST}}{}^2}{\beta_{\mathrm{ID\_min}}} \varepsilon_x \sigma_\delta^2 \right)^{1/2}, \tag{23}$$

where

$$\varepsilon_x = \frac{C_q \gamma^2}{J_{x0}} \frac{I_5 + \frac{4}{3\pi} \frac{\eta_{x\_\mathrm{ST}}{}^2}{\beta_{\mathrm{ID\_min}}} \frac{N_{\mathrm{ID}} L_{\mathrm{ID}}}{\rho_{\mathrm{ID}}^3}}{I_2 + \frac{1}{J_{x0}} \frac{N_{\mathrm{ID}} L_{\mathrm{ID}}}{2\rho_{\mathrm{ID}}^2}}, \tag{24}$$

$$\sigma_\delta{}^2 = \frac{C_q \gamma^2}{J_{E0}} \frac{I_3 + \frac{4}{3\pi} \frac{N_{\mathrm{ID}} L_{\mathrm{ID}}}{\rho_{\mathrm{ID}}^3}}{I_2 + \frac{2}{J_{E0}} \frac{N_{\mathrm{ID}} L_{\mathrm{ID}}}{2\rho_{\mathrm{ID}}^2}}. \tag{25}$$

Since the ID gaps can be adjusted independently of each other, we next determined the condition that minimizes the change in effective emittance when each ID field (the radius of curvature corresponding to the peak field) is varied within the operating range. As shown schematically in Fig. 1, the objective function for optimization is defined as the sum of the squares of the differences in the effective emittance at all points, composed of the two points at both ends defining the operating range and the other points dividing the defined range:

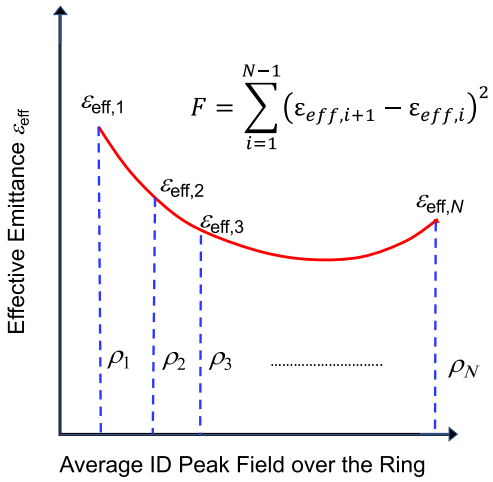

FIG. 1. Definition of the objective function F and division of the operational range of IDs.

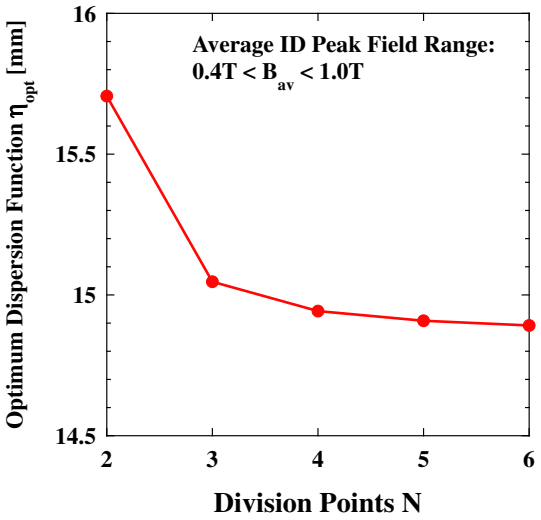

FIG. 2. The dependence of the optimum dispersion function η_{opt} on the number of divisions obtained from Eq. (27) when the natural emittance is 115 pmrad. N on the horizontal axis is the maximum number of division points: $N = 2, 3, 4, \ldots$ corresponding to the case where the number of divisions is $1, 2, 3, \ldots$, respectively.

$$F = \sum_{i=1}^{N-1} (\varepsilon_{\mathrm{eff},i+1} - \varepsilon_{\mathrm{eff},i})^2. \tag{26}$$

Then, the condition that minimizes the change in the effective emittance over the operating range of IDs is expressed as

$$\frac{\partial F}{\partial \eta_{x\_\mathrm{ST}}} = \frac{\partial}{\partial \eta_{x\_\mathrm{ST}}} \sum_{i=1}^{N-1} (\varepsilon_{\mathrm{eff},i+1} - \varepsilon_{\mathrm{eff},i})^2 = 0. \tag{27}$$

The optimum value of $\eta_{x\_\mathrm{ST}}(\equiv \eta_{\mathrm{opt}})$ is obtained by solving Eq. (27).

Figure 2 shows an example of the dependence of the optimum dispersion on the number of divisions. The optimum dispersion is calculated by assuming 115 pmrad as a natural emittance (see Table I, below) and assuming that the average peak field varies from 0.4 to 1 T by the independent tuning of the IDs. As can be seen from this figure, if the dependence of the effective emittance on the peak field (or gap) of IDs is smooth, the optimum dispersion converges quickly with the increase in the number of divisions. The dependence on the number of divisions becomes more pronounced as the natural emittance increases and the operating range of IDs widens. In this paper, we will discuss the case where the emittance is equal to or less than 115 pmrad and the range of the average ID field is equal to or narrower than a range from 0.4 to 1 T. Under these conditions, it is sufficient to divide the operating range into two parts and set $N = 3$ to evaluate the optimum value of the dispersion η_{opt}.

When the number of divisions is 2 ($N = 3$), the optimum condition is specified by the following equations:

$$F = F_1 + F_2 = (\varepsilon_{\mathrm{eff},2} - \varepsilon_{\mathrm{eff},1})^2 + (\varepsilon_{\mathrm{eff},3} - \varepsilon_{\mathrm{eff},2})^2, \tag{28}$$

TABLE I. Parameters used in the calculation.

Ring parameters	Lattice	44 normal cells + 4 straight cells
	Cell structure	5BA
	Stored beam energy E [GeV]	6
	Lorentz factor γ	11742
	Betatron tunes (ν_x, ν_y)	(108.100, 42.580)
	Energy spread σ_δ [%]	0.102
	Natural emittance ε_{x0} [pmrad]	115
	Momentum compaction factor α	3.902×10^{-5}
	Damping partition numbers, $J_x/J_y/J_E$	1.299/1.000/1.701
	Radiation integral I_1 [m]	5.134×10^{-2}
	Radiation integral I_2 [m^{-1}]	0.1635
	Radiation integral I_3 [m^{-2}]	5.438×10^{-3}
	Radiation integral I_4 [m^{-1}]	-4.884×10^{-2}
	Radiation integral I_5 [m^{-1}]	4.637×10^{-7}
ID parameters	Undulator period [mm]	22
	Number of periods	160
	Number of undulators	34
	β_x at the center of undulator straight [m]	6.1
	α_x at the center of undulator straight [–]	0.0
	Initial dispersion functions, η[m]/η'[–] at the center of undulator straight	0.0/0.0

$$\frac{\partial F}{\partial \eta_{x\_ST}} = \frac{\partial F_1}{\partial \eta_{x\_ST}} + \frac{\partial F_2}{\partial \eta_{x\_ST}} = 0. \tag{29}$$

The explicit expressions of $\frac{\partial F_1}{\partial \eta_{x\_ST}}$ and $\frac{\partial F_2}{\partial \eta_{x\_ST}}$ can be obtained in a straightforward manner and are given in the Appendix. The optimum value of the dispersion function η_{opt} can be obtained numerically by solving Eq. (29).

III. VALIDITY OF THE OPTIMUM CONDITION

In this section, we evaluate the effectiveness of the optimization procedure above. To this end, we take the SPring-8-II [11] lattice as an example and calculate the optimum value of the dispersion function. The parameters used in the calculation, as listed in Table I, have been updated from the data provided in the SPring-8-II conceptual design report [11]. Under the achromatic condition, the natural emittance is 115 pmrad.

During the independent tuning, the gap of each ID can be varied according to the specific requirements of the experimental users. We assume that the average value of the ID peak magnetic field over the whole storage ring varies in the region ranging from 0.4 to 1 T. In this case, with $N = 3$, the evaluation points of the undulator field are $B_1 = 0.4$ T, $B_2 = 0.7$ T, and $B_3 = 1$ T, and the corresponding radii of curvature at the beam energy of 6 GeV are $\rho_1 = 50.035$ m, $\rho_2 = 28.591$ m, and $\rho_3 = 20.014$ m, respectively. Under these conditions, the objective function F is calculated with Eq. (28), and its dependence on η_{x_ST} is shown in Fig. 3(a). From this figure, it can be seen that for the achromatic optics, i.e., $\eta_{x\_ST} = 0$, the objective function F takes a local maximum, and, as the dispersion η_{x_ST} increases, the value of F decreases and it takes a minimum value at $\eta_{x\_ST} = 15.0$ mm$(\equiv \eta_{\mathrm{opt}})$. Furthermore, since F is an even function of η_{x_ST}, we can say that it always gives a local maximum at $\eta_{x\_ST} = 0$ and takes a minimum value at a nonzero dispersion value of $\pm|\eta_{\mathrm{opt}}|$. The partial derivative of the objective function with respect to the dispersion, $\partial F/\partial \eta_{x\_ST}$, is calculated from Eq. (29), and its dependence on η_{x_ST} is as shown in Fig. 3(b). We obtain an optimum value of the dispersion $\eta_{\mathrm{opt}} = 15.0$ mm as a real number solution of $\partial F/\partial \eta_{x\_ST} = 0$, where the objective function F is minimized.

Next, we use the obtained optimum value of η_{opt} to determine the extent to which the variations of the emittance ε_x and the effective emittance $\varepsilon_{\mathrm{eff}}$ can be suppressed during the independent tuning of the IDs. Figure 4 shows the variation of ε_x and $\varepsilon_{\mathrm{eff}}$ as a function of the average peak field of the IDs for different values of η_{x_ST} ranging from 0 to 25 mm in 5 mm increments, including $\eta_{\mathrm{opt}} = 15.0$ mm. The region highlighted in yellow indicates the ID operating range where the average peak field of the IDs is between 0.4 and 1 T. From Fig. 4(b), we see that, in the achromatic case with $\eta_{x\_ST} = 0$, the effective emittance $\varepsilon_{\mathrm{eff}}$ varies by 50% in average from 100 to 60 pmrad during independent tuning. By optimizing the quasiachromatic condition (i.e., by setting η_{x_ST} to $\eta_{\mathrm{opt}} = 15.0$ mm), the change in $\varepsilon_{\mathrm{eff}}$ is limited to only a variation of 6% in average from 124 to 117 pmrad. By comparing the curves shown for the different η_{x_ST} values, we can confirm that the variation is actually minimized at η_{opt}. It is clear from Fig. 4(a) that, when the dispersion takes the optimum

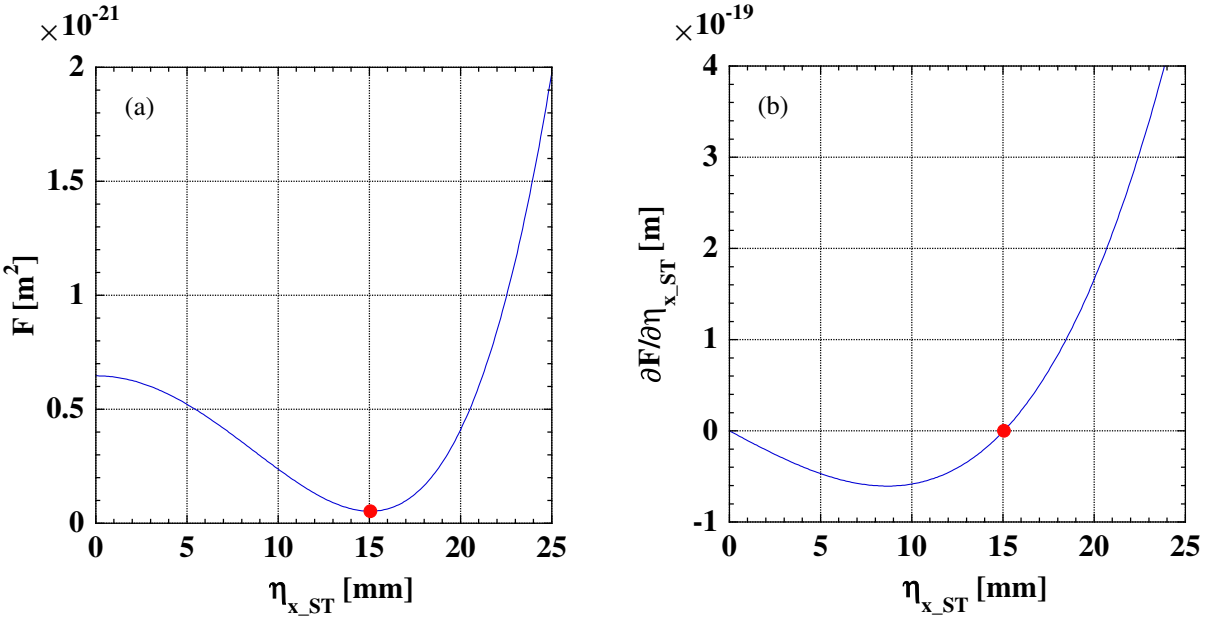

FIG. 3. Objective function F (a) and its derivative with respect to the dispersion function η_{x_ST} (b) for the case of $N = 3$. The red dots indicate the local minimum point where $\frac{\partial F}{\partial \eta_{x\_ST}} = 0$.

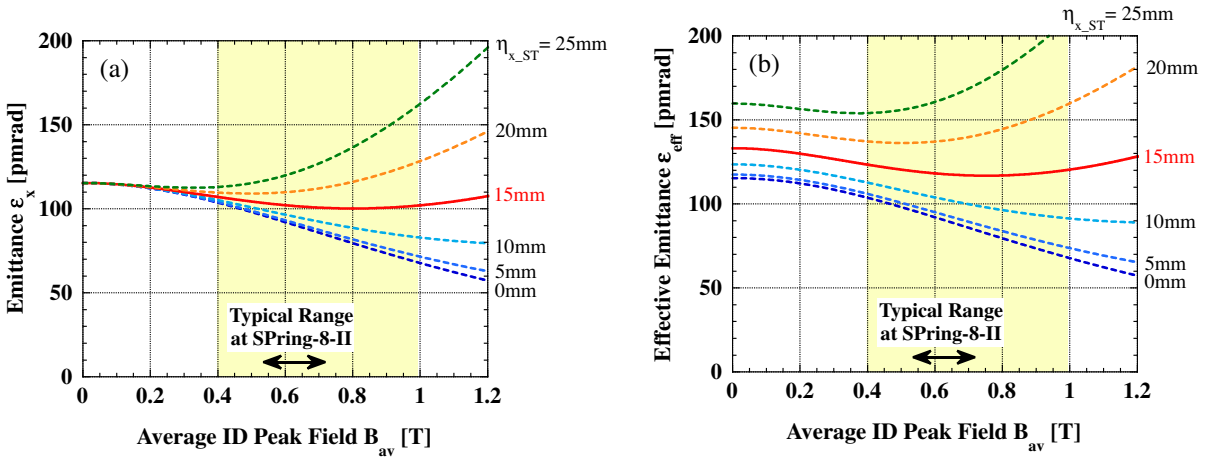

FIG. 4. Dependence of emittance (a) and effective emittance (b) on the average ID peak field for a given value of the dispersion η_{x_ST} leaked into the straight section. The red solid curves show the minimized variations by the optimum value of $\eta_{\mathrm{opt}} = 15.0$ mm. The black arrows represent a typical range of B_{av} (0.54 T $\leq B_{av} \leq$ 0.74 T) expected at SPring-8-II (see the next section for details).

value η_{opt}, the variation of not only the effective emittance, but also the emittance itself is minimized.

IV. SUPPRESSION OF EMITTANCE VARIATION UNDER THE OPTIMUM QUASIACHROMATIC CONDITION

In the previous sections, we proposed a method for partially suppressing variation of the effective emittance by optimizing the quasiachromatic condition. In this section, by using the SPring-8-II lattice parameters listed in Table I, we systematically investigate how the suppression performance depends on the natural emittance or on the imposed independent tuning conditions.

A. Dependence on natural emittance

To study the dependence on the natural emittance, we intentionally changed the radiation integral I_5 in Table I and gradually lowered the natural emittance from 115 to 100, 70, 50, 30, and 10 pmrad. In this way, we prepared six different optic configurations and calculated the emittance variation under the optimized quasiachromatic condition. For comparison, we also calculated the emittance variation under the achromatic condition in each of the optic configurations. The results are shown in Fig. 5. In these calculations, the average ID peak magnetic field B_{av} was assumed to vary between 0.4 and 1.0 T during the independent tuning in user operations.

Even when the natural emittance is 10 pmrad, Fig. 5(a) shows that the dispersion leakage in the straight section is about 4 mm, which is well within the range of control. As can be seen from Fig. 5(b), the natural emittance variation is approximately 40% in the achromatic case (red circles) in the range from 10 to 115 pmrad. On the other hand, under the optimized quasiachromatic condition, the emittance variation is well suppressed to approximately 6% (blue

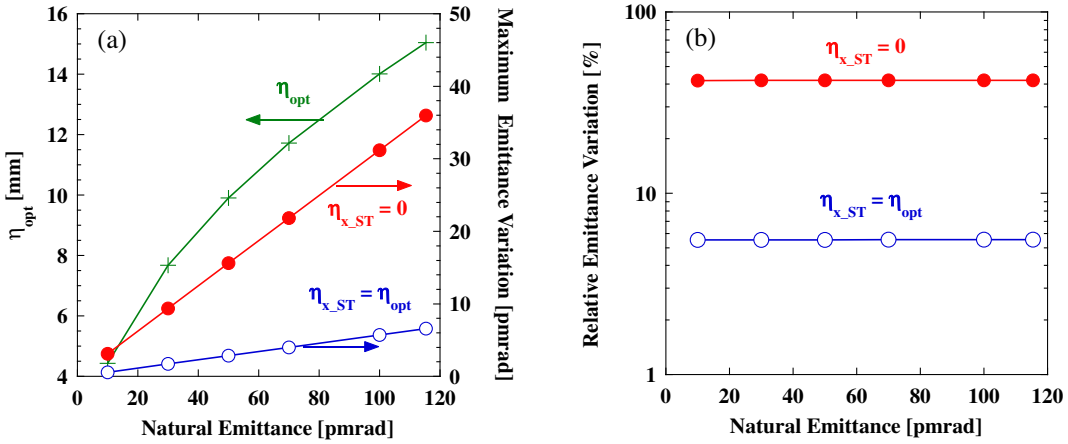

FIG. 5. Dependences of the suppression effect of emittance variation on natural emittance. The maximum (a) and relative (b) values of emittance variation are plotted. The red filled and blue open circles show calculation results under the achromatic and optimized quasiachromatic conditions, respectively. The green crosses in Fig. 5(a) show values for the optimum linear energy dispersion η_{opt} at the straight section under the quasiachromatic condition.

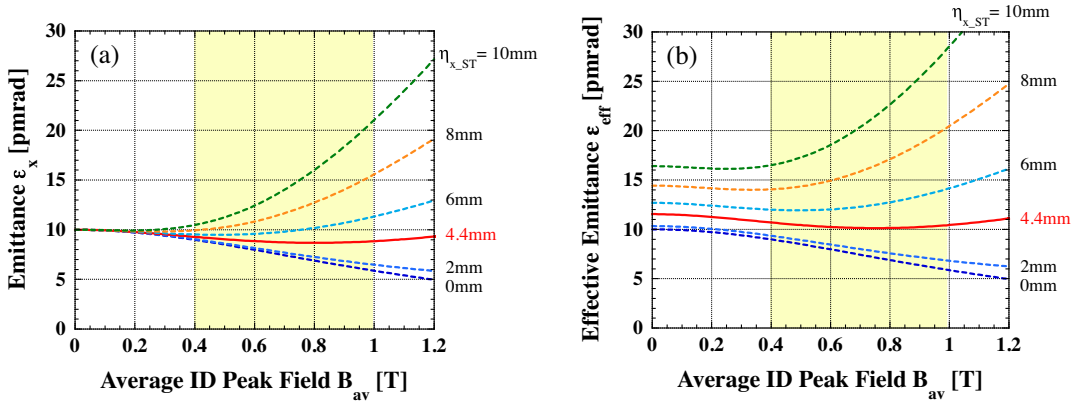

FIG. 6. The same as Fig. 4 but for the natural emittance of 10 pmrad.

circles) in the same range. Figure 6 shows the emittance variation with respect to the average ID peak field in the case of 10 pmrad natural emittance. Even for an ultralow emittance ring, the emittance variation is greatly reduced with the optimized dispersion leakage of 4.4 mm.

B. Dependence on the range of independent tuning

The gaps are opened or closed and other ID parameters are adjusted according to specific experimental requirements at each beam line. Since the ring conditions differ each time, the changes are not systematic. The variation range of the average magnetic field of IDs over the whole ring is an important parameter, which governs the radiation damping of the ring. This value is expected to differ for each synchrotron radiation source. Here, we investigate how the operating range of the average ID field affects the suppression of the effective emittance variation.

Using the example of the present 8 GeV storage ring SPring-8 [12], we first investigated how much the average peak field B_{av} actually varies during user experiments. Thirteen in-vacuum planar undulators with relatively frequent gap movements were selected, and the variation of B_{av} was evaluated from their gap values over ten days. We applied the following averaging procedure. We first calculated the peak magnetic field from the gap value every minute for each ID at SPring-8. Then, we converted the magnetic field so that the photon energy being used remained constant at SPring-8-II (see Table I for assumed ID parameters and beam energy). We finally calculated the rms of the obtained field values $B_{0,i}$ $(i = 1, ..., N_{\mathrm{ID}})$ and

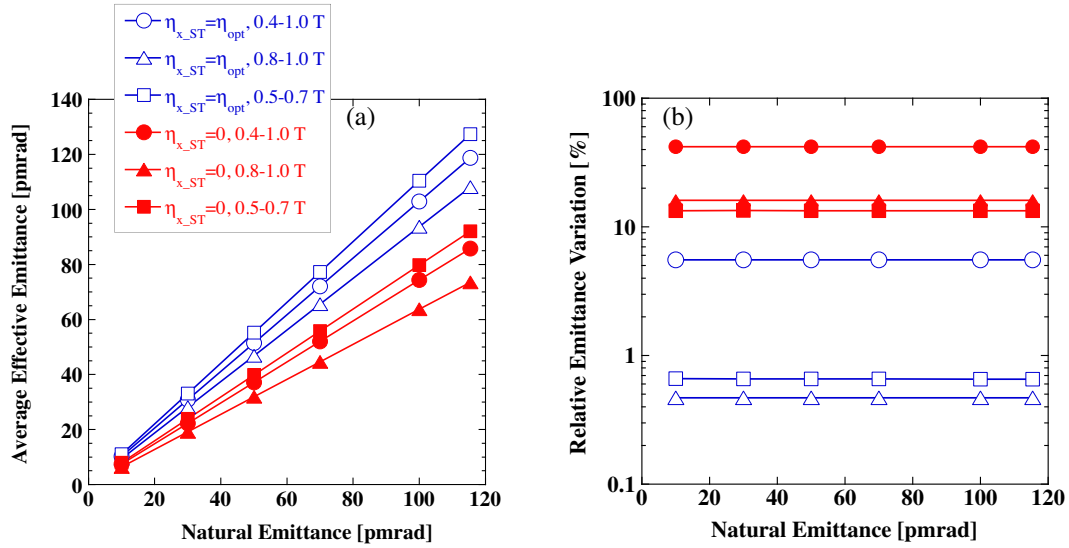

FIG. 7. Dependence of the average effective emittance (a) and suppression effect of emittance variation (b) on the operating range of B_{av}. The vertical axis in the left figure represents the average of the effective emittance taken over a given range of B_{av}, and that in the right figure represents the normalized maximum variation of the effective emittance in the same range of B_{av}. The red filled circles, triangles, and squares indicate calculations under the achromatic condition for the ranges of 0.4 T $\leq B_{av} \leq$ 1.0 T, 0.8 T $\leq B_{av} \leq$ 1.0 T, and 0.5 T $\leq B_{av} \leq$ 0.7 T, respectively. The blue open circles, triangles, and squares indicate calculations under the optimized quasiachromatic condition for the ranges of 0.4 T $\leq B_{av} \leq$ 1.0 T, 0.8 T $\leq B_{av} \leq$ 1.0 T, and 0.5 T $\leq B_{av} \leq$ 0.7 T.

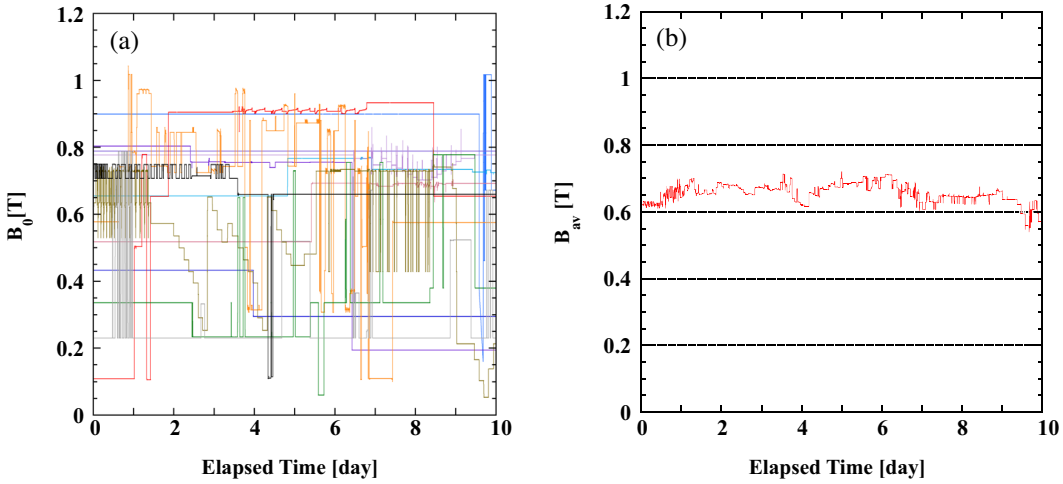

FIG. 8. The variation of the peak magnetic field of thirteen undulators over ten days of user operation (a) and their average (b). The ID gap data for the present SPring-8 ring is scaled to the SPring-8-II ring, and the peak magnetic field is calculated.

took it as an average field $B_{av}(=\sqrt{\sum_i B_{0,i}^2/N_{\mathrm{ID}}})$, finding the result for the 13 undulators to be 0.656 T, and the maximum and minimum values were 0.720 and 0.540 T, respectively. The distribution of the average field was relatively coherent and single peaked, with a standard deviation of 0.0287 T (see Fig. 8). Based on these statistical results, we selected 0.5 T $\leq B_{av} \leq$ 0.7 T as a more realistic operating range of B_{av} during the independent tuning in user operations. Also, another operating range, 0.8 T $\leq B_{av} \leq$ 1.0 T, was selected to determine how the range width and average field value affected performance.

With the operating ranges thus reduced to about 1/3 having the different central B_{av} values, we reoptimized the quasiachromatic conditions and evaluated how the emittance variation was suppressed for two cases: 0.8 T $\leq B_{av} \leq$ 1.0 T and 0.5 T $\leq B_{av} \leq$ 0.7 T. Figure 7 shows the average effective emittances and their variations for the three cases under the optimized quasiachromatic condition. The figure also shows the respective values for the achromatic condition as a reference. Note that, for the narrower range cases, the maximum variations of the effective emittance were reduced to only 0.5%–0.7%. Since the variation range of B_{av} was narrowed, the deviation in the achromatic cases also became smaller (16%–13%) but was tens of times larger than in the optimized quasiachromatic case.

It is also noteworthy that the effective emittance itself cannot be reduced by narrowing the operating range. For example, if the natural emittance is 100 pmrad, the average effective emittance is increased to about 110 pmrad when the operating range of B_{av} is narrowed to 0.5 T $\leq B_{av} \leq$ 0.7 T. On the other hand, when the operating range of B_{av} is set to 0.8 T $\leq B_{av} \leq$ 1.0 T with the same width, the optimum dispersion becomes smaller and the average effective emittance is about 94 pmrad. This emittance reduction is due to the high B_{av} over the operating range.

From these results, we see that utilizing the proposed method most effectively requires setting an appropriate operating range for the average ID peak field B_{av} during the independent tuning. In addition, the IDs not being used for experiments should be operated with the gaps as closed as possible. This enables a lower effective emittance by increasing the average ID peak field.

C. Validity of the concept of average magnetic field

As explained in the previous subsection, we sampled the gap values of 13 in-vacuum planar undulators used in the present SPring-8 storage ring. Figure 8(a) shows the variation

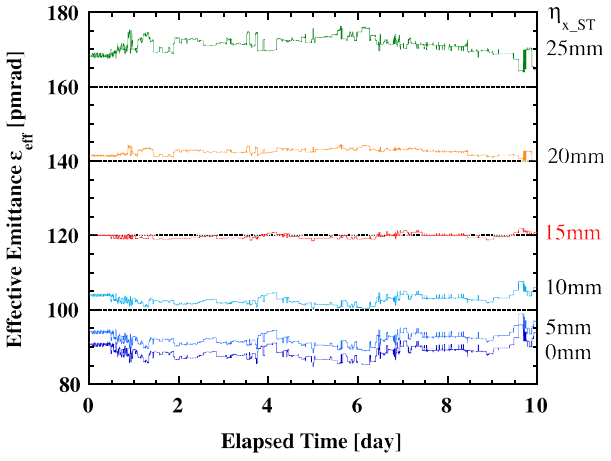

FIG. 9. The variation of the effective emittance for several values of the dispersion leakage. The peak field data in Fig. 8(a) are used in the calculation. The standard deviations for $\eta_{x\_ST} = 0$, 5, 10, 15, 20, and 25 mm are, respectively, 1.8, 1.7, 1.3, 0.6, 0.8, and 2.1 pmrad. The standard deviation is minimized with the optimized dispersion leakage of 15 mm.

of the peak magnetic field deduced from collected gap data over ten days of user operation. We also show the trend of their average value in Fig. 8(b). From the figure, the average peak field B_{av} is 0.720 T at the maximum, 0.540 T at the minimum, and typically 0.656 T. While the peak field of each ID is widely distributed [Fig. 8(a)], the average field B_{av} is limited to a certain narrow range, which justifies the introduction of an average peak magnetic field.

In our approach, the concept of the average magnetic field is used to optimize the dispersion leakage η_{x_ST}. Here, we evaluate the variation of the effective emittance with several values of η_{x_ST} directly from the field data of each ID during an actual user operation period as shown in Fig. 8(a). Figure 9 shows the trend of the effective emittance for several values of the dispersion leakage. We see that the emittance variation is minimized with the optimized dispersion leakage of 15 mm. Thus, the introduction of an average magnetic field is justified during the optimization process.

V. SUMMARY

Emittance variation presents a major obstacle for conducting precise experiments. We proposed a method to optimize the quasiachromatic condition in order to significantly reduce emittance variation during the independent tuning of IDs in extremely low emittance light source storage rings. Since this method is passive and does not require any special equipment, it can easily be implemented in any light source storage ring. We found that, with this method, the emittance variation can be reduced by an order of magnitude when compared to the usual achromatic case. We also demonstrated that the emittance variation can be reduced to less than 1% by carefully optimizing an operating range of the average ID peak field in consideration of the actual independent tuning of the IDs. We finally note that, since the amount of the required dispersion leakage is small, its impact on the lattice design and beam dynamics (e.g., lattice symmetry, dynamic aperture, momentum acceptance, intrabeam scattering, synchro-beta coupling, beam injection scheme, etc.) is expected to be insignificant, though these should be examined and optimized carefully in designing the lattice.

APPENDIX: DERIVATIVE OF OBJECTIVE FUNCTION F_i

In this Appendix, we give explicit expressions of $\frac{\partial F_1}{\partial \eta_{x\_ST}}$ and $\frac{\partial F_2}{\partial \eta_{x\_ST}}$ that are used to solve Eq. (29) for finding an optimum value of the dispersion function η_{opt}. Starting from Eqs. (23)–(25) and doing a few calculations, we obtain the following result ($i = 1, 2$):

$$
\begin{aligned}
\frac{\partial F_i}{\partial \eta_{x\_ST}} &= \frac{\partial(\varepsilon_{\mathrm{eff},i+1} - \varepsilon_{\mathrm{eff},i})^2}{\partial \eta_{x\_ST}} \\
&= \left(\frac{16}{3\pi}\varepsilon_{x,i}\frac{C_q\gamma^2}{J_{x0}}\frac{\frac{\eta_{x\_ST}}{\beta_{\mathrm{ID\_min}}}\frac{N_{\mathrm{ID}}L_{\mathrm{ID}}}{\rho_i^3}}{I_2 + \frac{1}{J_{x0}}\frac{N_{\mathrm{ID}}L_{\mathrm{ID}}}{2\rho_i^2}} + \frac{2\eta_{x\_ST}}{\beta_{\mathrm{ID\_min}}}\varepsilon_{x,i}\sigma_{\delta,i}^2 + \frac{8}{3\pi}\frac{C_q\gamma^2}{J_{x0}}\frac{{\eta_{x\_ST}}^3}{{\beta_{\mathrm{ID\_min}}}^2}\frac{\frac{N_{\mathrm{ID}}L_{\mathrm{ID}}}{\rho_i^3}}{I_2 + \frac{1}{J_{x0}}\frac{N_{\mathrm{ID}}L_{\mathrm{ID}}}{2\rho_i^2}}\sigma_{\delta,i}^2\right) \\
&\quad \times \left\{1 - \left({\varepsilon_{x,i}}^2 + \frac{{\eta_{x\_ST}}^2}{\beta_{\mathrm{ID\_min}}}\varepsilon_{x,i}\sigma_{\delta,i}^2\right)^{-1/2}\left({\varepsilon_{x,i+1}}^2 + \frac{{\eta_{x\_ST}}^2}{\beta_{\mathrm{ID\_min}}}\varepsilon_{x,i+1}\sigma_{\delta,i+1}^2\right)^{1/2}\right\} \\
&\quad + \left(\frac{16}{3\pi}\varepsilon_{x,i+1}\frac{C_q\gamma^2}{J_{x0}}\frac{\frac{\eta_{x\_ST}}{\beta_{\mathrm{ID\_min}}}\frac{N_{\mathrm{ID}}L_{\mathrm{ID}}}{\rho_{i+1}^3}}{I_2 + \frac{1}{J_{x0}}\frac{N_{\mathrm{ID}}L_{\mathrm{ID}}}{2\rho_{i+1}^2}} + \frac{2\eta_{x\_ST}}{\beta_{\mathrm{ID\_min}}}\varepsilon_{x,i+1}\sigma_{\delta,i+1}^2 + \frac{8}{3\pi}\frac{C_q\gamma^2}{J_{x0}}\frac{{\eta_{x\_ST}}^3}{{\beta_{\mathrm{ID\_min}}}^2}\frac{\frac{N_{\mathrm{ID}}L_{\mathrm{ID}}}{\rho_{i+1}^3}}{I_2 + \frac{1}{J_{x0}}\frac{N_{\mathrm{ID}}L_{\mathrm{ID}}}{2\rho_{i+1}^2}}\sigma_{\delta,i+1}^2\right) \\
&\quad \times \left\{1 - \left({\varepsilon_{x,i}}^2 + \frac{{\eta_{x\_ST}}^2}{\beta_{\mathrm{ID\_min}}}\varepsilon_{x,i}\sigma_{\delta,i}^2\right)^{1/2}\left({\varepsilon_{x,i+1}}^2 + \frac{{\eta_{x\_ST}}^2}{\beta_{\mathrm{ID\_min}}}\varepsilon_{x,i+1}\sigma_{\delta,i+1}^2\right)^{-1/2}\right\}. \qquad \text{(A1)}
\end{aligned}
$$

[1] D. Einfeld, J. Schaper, and M. Plesko, Design of a diffraction limited light source (DIFL), in *Proceedings of PAC1995* (1995), p. 177.

[2] EBS Storage Ring Technical Report, 2018, https://www.esrf.fr/about/upgrade; P. Raimondi, N. Carmignani, L. R. Carver, J. Chavanne, L. Farvacque, G. Le Bec, D. Martin, S. M. Liuzzo, T. Perron, and S. White, Commissioning of the hybrid multibend achromat lattice at the European Synchrotron Radiation Facility, Phys. Rev. Accel. Beams **24**, 110701 (2021).

[3] F. Sannibale, S. C. Leemann, H. Nishimura, D. Robin, C. Steier, C. Sun, and M. Venturini, Compensation of

insertion device induced emittance variations in ultralow emittance storage rings, in *Proceedings of IPAC2018* (2018), p. 1751.

[4] H. Wiedemann, *Particle Accelerator Physics*, 4th ed. (Springer, New York, 2015), Sec. 11.6.

[5] M. Masaki and S. Takano, Two-dimensional visible synchrotron light interferometry for transverse beam-profile measurement at the SPring-8 storage ring, J. Synchrotron Radiat. **10**, 295 (2003).

[6] Cyrille Thomas, Guenther Rehm, Ian Martin, and Riccardo Bartolini, X-ray pinhole camera resolution and emittance measurement, Phys. Rev. Accel. Beams **13**, 022805 (2010).

[7] S. Takano, M. Masaki, and H. Sumitomo, Recent progress in x-ray emittance diagnostics at SPring-8, in *Proceedings of IBIC2015* (2015), p. 283.

[8] F. Sannibale, M. P. Ehrlichman, T. Hellert, S. C. Leemann, D. Robin, C. Steier, C. Sun, and M. Venturini, Compensation of insertion device induced emittance variations in ultralow emittance storage rings by a dispersion bump in a wiggler, in *Proceedings of IPAC2019* (2019), p. 1627.

[9] D. Hidas, T. Shaftan, and T. Tanabe, Emittance and energy spread compensation for current and future low emittance synchrotron light sources, Phys. Rev. Accel. Beams **24**, 081601 (2021).

[10] H. Tanaka and A. Ando, Minimum effective emittance in synchrotron radiation sources composed of modified Chasman-Green lattice, Nucl. Instrum. Methods Phys. Res., Sect. A **369**, 312 (1996).

[11] SPring-8-II Conceptual Design Report, 2014, http://rsc.riken.jp/pdf/SPring-8-II.pdf.

[12] H. Kamitsubo, 8-GeV synchrotron radiation facility project in Japan: JAERI-RIKEN SPring-8 project, Nucl. Instrum. Methods Phys. Res., Sect. A **303**, 421 (1991); http://www.spring8.or.jp/en/.